Bulgarian Chemical Communications, Volume 50 Special Issue D (pp. 31 – 38) 2018

A Perspective on the Role of the Three-Phase Boundary in Solid Oxide Fuel Cell Electrodes

A. Bertei[1,2*], E. Ruiz-Trejo[2], D. Clematis[3], M. P. Carpanese[3], A. Barbucci[3], C. Nicolella[1], N. Brandon[2]

[1]*Department of Civil and Industrial Engineering, University of Pisa, Largo Lucio Lazzarino 2, 56122 Pisa, Italy*
[2]*Department of Earth Science and Engineering, Imperial College London, Prince Consort Road, SW7 2AZ London, UK*
[3]*Department of Civil, Chemical and Environmental Engineering, University of Genova, Via Montallegro 1, 16145 Genova, Italy*

Received May 14, 2018 Revised July 24, 2018

To the memory of Prof. Zdravko Stoynov

Within composite electrodes for solid oxide fuel cells (SOFCs), electrochemical reactions take place in the proximity of the so-called three-phase boundary (TPB), the contact perimeter where the electron-conducting, the ion-conducting and the porous phases meet. Strictly speaking, the TPB is a line and efforts have been made to increase its length per unit of electrode volume in order to reduce the activation losses. In this communication, by integrating physically-based modelling, 3D tomography and electrochemical impedance spectroscopy (EIS), a renovated perspective on electrocatalysis in SOFCs is offered, showing that the electrochemical reactions take place within an extended region around the geometrical TPB line. Such an extended region is in the order of 4 nm in Ni/$Sc_{0.2}Zr_{0.9}O_{2.1}$ (Ni/ScSZ) anodes while approaches hundreds of nanometres in $La_{0.8}Sr_{0.2}MnO_{3-x}$/$Y_{0.16}Zr_{0.92}O_{2.08}$ (LSM/YSZ) cathodes. These findings have significant implications for preventing the degradation of nanostructured anodes, which is due to the coarsening of the fractal roughness of Ni nanoparticles, as well as for the optimisation of composite cathodes, indicating that the adsorption and surface diffusion of oxygen limit the rate of the oxygen reduction reaction (ORR). In both anodes and cathodes, the results point out that the surface properties of the materials are key in determining the performance and lifetime of SOFC electrodes.

Key words: Solid oxide fuel cells, modelling, 3D tomography, degradation, electrochemical impedance spectroscopy, electrocatalysis

INTRODUCTION

Solid oxide fuel cells (SOFCs) are energy devices which produce electric power from the direct electrochemical conversion of a fuel, such as hydrogen. A SOFC consists of two porous electrodes, namely the cathode, which hosts the oxygen reduction reaction, and the anode, wherein fuel oxidation takes place [1]. The electrodes are separated by a dense ceramic electrolyte wherein oxygen ions, produced at the cathode, migrate towards the anode (Figure 1a).

SOFC can be used in reverse mode (Solid oxide electrolyzer cells, SOECs), to produce hydrogen. Then, innovative designs are also developed in the literature, based on properties of a mixed anionic and protonic conductor used as central membrane [2-6], or of electrolyte supported cells in symmetrical configuration [7] to improve operation as reversible solid oxide cells.

In composite electrodes, the cathodic and anodic electrochemical reactions involve gaseous species (i.e., H_2, O_2 and H_2O), electrons (e^-) and oxygen ions (O^{2-}) as follows:

$$\frac{1}{2}O_{2(g)} + 2e^-_{(el)} \leftrightarrow O^{2-}_{(io)} \quad (1)$$

$$H_{2(g)} + O^{2-}_{(io)} \leftrightarrow H_2O_{(g)} + 2e^-_{(el)} \quad (2)$$

These electrochemical reactions involve transport of neutral and charged species within different phases, namely the pores, the electron-conducting phase (*el*) and the ion-conducting phase (*io*). In both the cathode and the anode these electrochemical reactions are typically assumed to take place at the three-phase boundary (TPB), which is the contact perimeter among the electron-conducting, the ion-conducting and the pore phases, where both reactants and products can co-exist [8] (Figure 1b). This assumption effectively implies that the reactions take place along a mono-

To whom all correspondence should be sent:
E-mail: antonio.bertei@unipi.it

dimensional line, namely the TPB line. Following this assumption, efforts have been made in the past in order to maximise the TPB length per unit volume in both the electrodes to speed up the rate of electrochemical conversion and thus lower the electrode activation resistance [9-11].

However, generally catalysis and electrocatalysis indicate that heterogeneous reactions take place at the bi-dimensional interface between different phases, thus not along a mono-dimensional line. Therefore, also in SOFC electrodes the reaction zone must spread within an extended region around the geometrical TPB line.

This perspective article summarises the efforts of the authors in determining the lateral extension and the role of the TPB in both SOFC anodes [12] and cathodes [13-15] by combining experimental techniques, such as electrochemical impedance spectroscopy (EIS) and focused ion beam-SEM (FIB-SEM) tomography, as well as physics-based modelling. Rather than focusing on the details of the investigations, which can be found in a series of papers already published by the authors [12-15], this communication summarises the key findings and their practical implications in order to give a holistic overview of the role of the TPB in SOFC electrocatalysis.

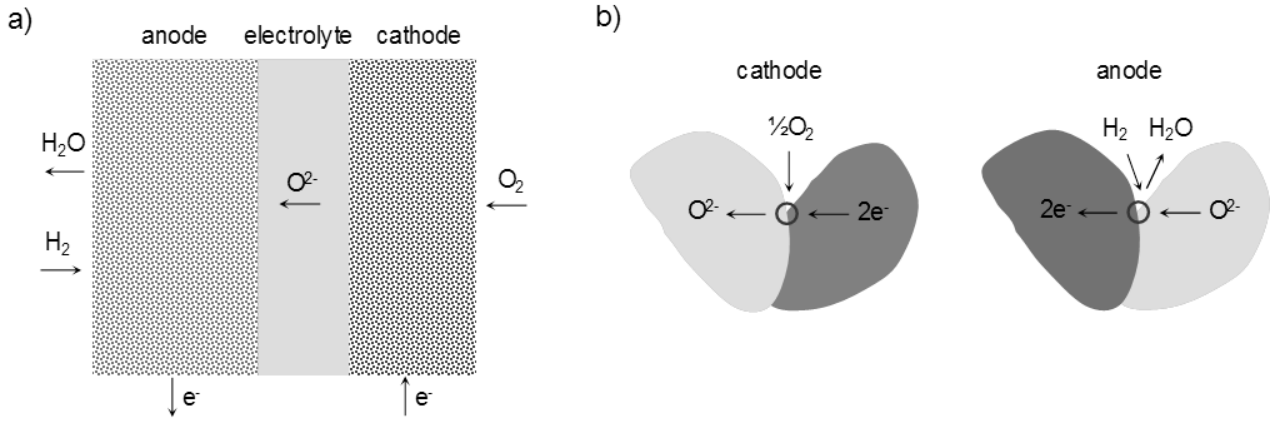

Fig. 1. a) Schematic representation of a solid oxide fuel cell. b) Cathodic and anodic reactions assumed to occur at the three-phase boundary, denoted with a circle.

THE ROLE OF THE TPB AT THE CATHODE

Experimental

The oxygen reduction reaction (ORR, Eq. (1)) was investigated in cathodes made of strontium-doped lanthanum manganite ($La_{0.8}Sr_{0.2}MnO_{3-\delta}$, LSM), which is the electron-conducting electrocatalyst, and yttria-stabilized zirconia ($(Y_2O_3)_{0.08}(ZrO_2)_{0.92}$, YSZ), which is the ion-conducting electrolyte. In fact LSM, with LSCF and BSCF and YSZ with doped ceria are the state of art materials respectively for cathode and electrolyte [16-17]. Thin layers (~3 μm in thickness) of porous LSM were sintered on both sides of a YSZ disk as described by Carpanese et al. [14]. Special attention was paid on the geometrical requirements of the working, counter and reference electrodes in order to ensure reliable EIS measurements in the three-electrode setup. EIS, in fact, is very powerful technique to study SOFC, if the appropriate corrections are performed [18].

Impedance spectroscopy measurements were carried out within the frequency range 10^6–10^{-1} Hz with different oxygen partial pressures (0.10–0.21 atm) in the temperature range 700–800 °C. The cathodic bias was varied between 0.0 V (i.e., open-circuit conditions) and 0.4 V (i.e., strong cathodic bias). The electrode thickness and porosity as well as the LSM particle size were evaluated through SEM analysis.

Modelling

The EIS data were interpreted by using a mechanistic model of the ORR mechanism [13,15]. It was assumed that molecular oxygen undergoes a dissociative adsorption on the LSM surface, then oxygen adatoms diffuse along the electrocatalyst surface to reach the TPB at the LSM/YSZ interface, where the proper charge transfer occurs (Figure 2). Thus, the global reaction in Eq. (1) was decoupled into two elementary steps:

$$\frac{1}{2}O_{2(g)} \leftrightarrow O_{(el,s)} \tag{3a}$$

$$O_{(el,s)} + 2e^-_{(el)} \leftrightarrow O^{2-}_{(io)} \tag{3b}$$

where the subscript *el,s* refers to the LSM surface.

This elementary mechanism was modelled by applying the conservation of oxygen adatoms on the LSM surface, taking into account the Langmuir dissociative adsorption and the Fick surface diffusion as in Eq. (4). The charge transfer in Eq. (3b) was modelled according to a linearized Butler-Volmer kinetics as in Eq. (5):

$$\frac{\partial\theta}{\partial t} = D_s^{eff}\frac{\partial^2\theta}{\partial x^2} + k_{des}\left(K\cdot p_{O_2}\cdot(1-\theta)^2 - \theta^2\right) \qquad (4)$$

$$i_{TPB} = i_{00}\cdot\left(\frac{\theta_0}{1-\theta_0}\right)^{1-\alpha}\cdot\frac{2F}{RT}\cdot\left(\eta_{cat} - \frac{RT}{2F}\ln\left(\frac{\theta_{eq}}{\theta_0}\frac{1-\theta_0}{1-\theta_{eq}}\right)\right) \qquad (5)$$

In Eqs. (4) and (5) θ represents the surface coverage fraction of oxygen adatoms $O_{(el,s)}$ (where θ_0 and θ_{eq} refer to the coverage fraction at the LSM/YSZ interface and in equilibrium condition, respectively), k_{des} and K the kinetic and equilibrium constants of oxygen adsorption, D_s^{eff} the effective surface diffusion coefficient of oxygen adatoms, p_{O2} the oxygen partial pressure, i_{00} the exchange current density pre-factor, η_{cat} the applied cathodic bias, T the absolute temperature, F and R the Faraday and gas constants, respectively. For more details on model equations the reader is referred to Bertei et al. [15].

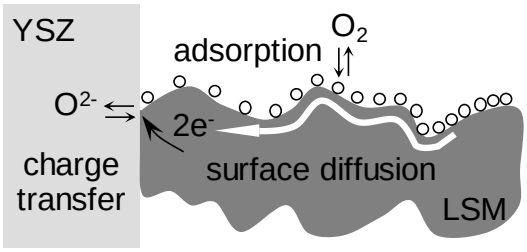

Fig.2. The proposed mechanism of the oxygen reduction reaction (ORR) in LSM/YSZ cathodes.

Results and interpretation

The mechanistic model in Eqs. (4) and (5) was used to fit experimental impedance spectra collected at different temperatures, oxygen partial pressures and cathodic bias [14]. The model was capable to reproduce the depressed shape of the cathode response as in Figure 3a, with minor deviations at low frequency likely due to possible heterogeneity of the electrode microstructure. The agreement between model and experimental results indicates that two contributions were present: a low-frequency feature, related to the coupled adsorption/surface diffusion process (i.e., Eq. (4)), and a medium-frequency feature, related to the charge transfer reaction at the TPB (i.e., Eq. (5)). In particular, simulations showed that the resistance of the charge transfer reaction was much smaller than the resistance associated to the adsorption/diffusion process, which represented the dominant resistance in the cathode (inset in Figure 3a).

In addition to reproducing the EIS behaviour, the model allowed for the prediction of the concentration profile of oxygen adsorbed on the surface of the electrocatalyst [15]. Figure 3b shows that the surface coverage of oxygen adatoms on the electrocatalyst surface differs from the equilibrium surface fraction in the proximity of the TPB, thus identifying the zone where adsorption and surface diffusion processes take place. The characteristic length of the adsorption/diffusion process was estimated as:

$$\delta = \sqrt{\frac{D_s}{2k_{des}\sqrt{Kp_{O_2}}}} \qquad (6)$$

which is equal to 0.2–0.3 μm within 700–800 °C. This value was found to hold also in composite LSM/YSZ cathodes, i.e., consisting of a mixture of LSM and YSZ particles, as reported by Fu et al. [13]. By varying the particle size, the authors showed that the cathode polarisation resistance scaled inversely with L_s/δ, where L_s is the semi-distance between two TPBs along the surface of an LSM particle (inset in Figure 3b).

Practical implications

The results summarised in the previous section imply that the characteristic length δ of the oxygen adsorption/diffusion process, equal to 0.2–0.3 μm, must be regarded as the effective width of the reaction zone around the geometrical TPB. Therefore, the oxygen reduction reaction does not take place along the mono-dimensional TPB line, rather, the rate-determining process (i.e., the adsorption and surface dissociation) extends for about 0.2–0.3 μm along the surface of the electrocatalyst. Such a lateral extension of the reaction zone can be neglected when LSM particles are bigger than 2–3 μm, that is, for $L_s/\delta >> 1$. However, when the particle size becomes comparable to the characteristic length δ, as in advanced electrodes produced via nanoparticle infiltration [19], the whole surface of the electrocatalyst nanoparticles may become active for the ORR, thus referring solely to the TPB as the reaction site would be meaningless.

Critically, this means that the surface properties of the electrocatalyst, such as the density of adsorption sites, the surface diffusion coefficient and the adsorption kinetic constant, are more

important than the increase in the TPB length because the charge transfer is not rate-limiting. In other words, the TPB length is not the only parameter to be maximised [15]. Rather, as also suggested by Banerjee and Deutschmann [20,21], research should focus on improving the adsorption and diffusion rates on the surface of the electrocatalyst.

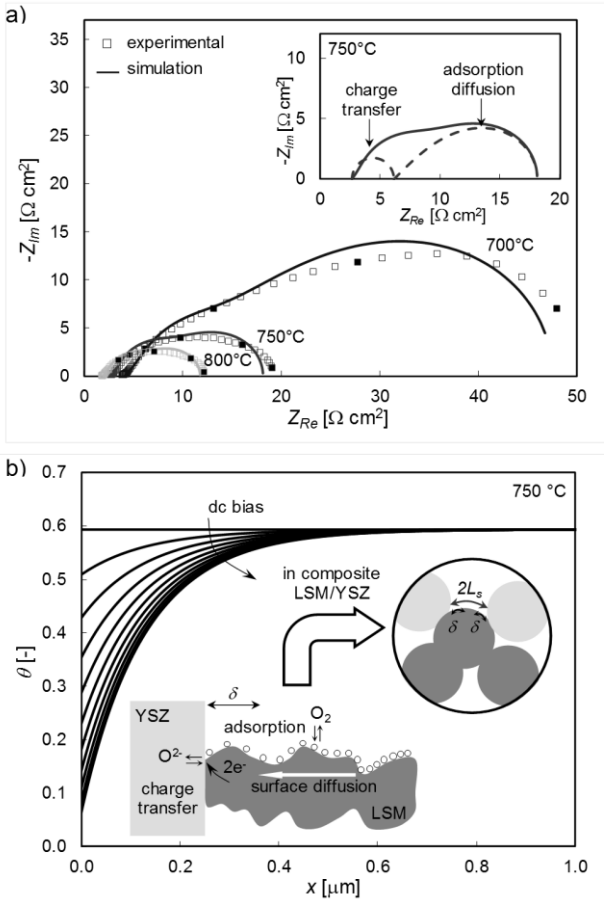

Fig 3. a) Fitting of the experimental EIS spectra of the porous LSM cathode at different temperatures (OCV, p_{O2} = 0.21 atm). The inset shows the deconvolution of the impedance in two contributions. b) Simulated profile of oxygen surface coverage along the LSM thickness. The insets show the extension δ of the adsorption/diffusion process in porous LSM and in composite LSM/YSZ cathodes compared to the semi-distance L_s between adjacent TPBs.

THE ROLE OF THE TPB AT THE ANODE

Experimental

The hydrogen oxidation reaction (Eq. (2)) was investigated in nanostructured anodes fabricated on the top of a YSZ disk. Scaffolds of scandia-stabilized zirconia ($(Sc_2O_3)_{0.10}(ZrO_2)_{0.90}$, ScSZ, i.e., the ion-conducting phase) were produced by tape casting and sintered at 1250 °C for 2 h as described elsewhere [12]. In fact, these are state-of-the art materials for SOFC, both in hydrogen and alternative fuels [16,22]. The electron-conducting phase was introduced within the scaffolds via multiple infiltrations of a 2 M $Ni(NO_3)_2$ ethanol solution followed by firing at 550 °C for 30 min to decompose the nitrate solution to NiO. The samples were finally fired in nitrogen at 750 °C for 30 min, then cooled at 550 °C where NiO was reduced to Ni in a 5% H_2/3% H_2O atmosphere.

The electrochemical degradation of the anodes was monitored continuously by using EIS within the frequency range 10^6–10^{-1} Hz at open circuit conditions, 550 °C in 5% H_2/3% H_2O atmosphere for up to 200 h. The anode microstructure was reconstructed ex-situ before and after degradation through FIB-SEM tomography [12]. A field emission gun-SEM (FEG-SEM) microscope was used to acquire images of the microstructure at higher magnification.

Modelling

The three-dimensional tomographic datasets were manually segmented in three phases (i.e., Ni, ScSZ and pore), allowing for the quantitative evaluation of the TPB length per unit volume L_{TPB} and the effective ionic conductivity σ_{io}^{eff} from the microstructural reconstructions [12,23].

A validated physically-based equivalent circuit [24] was adopted to deconvolve the impedance spectra and to relate the electrode charge transfer resistance R_{ct} to the microstructural properties:

$$R_{ct} = \sqrt{\frac{RT}{F}\frac{1}{i_0 L_{TPB}\sigma_{io}^{eff}}}\coth\left(\sqrt{h^2\frac{F}{RT}\frac{i_0 L_{TPB}}{\sigma_{io}^{eff}}}\right). \qquad (7)$$

where h is the electrode thickness and i_0 is the exchange current density of the hydrogen oxidation reaction. Notably, Eq. (7) assumes that the anodic charge transfer reaction takes place along the geometrical TPB line.

Hence, two independent estimations of the TPB density were obtained: one from the tomographic reconstruction of the anode microstructure, one through Eq. (7) from the charge transfer resistance evaluated from EIS data.

Results and interpretation

Figure 4a shows the evolution with time of the charge transfer resistance of the nanostructured Ni/ScSZ anode at 550 °C as obtained by the analysis of EIS data. Experimental results showed a rapid increase in charge transfer resistance within the first 100 h, followed by stabilisation [12,25]. Such a rapid increase in anode charge transfer resistance evidenced the presence of an electrochemical degradation mechanism affecting the hydrogen oxidation reaction (Eq. (2)).

Since the microstructure of the ScSZ scaffold can be considered stable at 550 °C, the increase in R_{ct} was attributed to a change in the active TPB length as a consequence of rearrangement of the Ni phase upon annealing [12]. Thus, Eq. (7) was used to estimate the temporal evolution of the TPB density from R_{ct}, as shown in Figure 4b. Figure 4b shows that the rapid increase in charge transfer resistance could be interpreted as a rapid decrease in TPB length per unit volume, followed by stabilisation (see line). However, Figure 4b shows that there was a mismatch between the TPB density estimated via EIS through Eq. (7) (line) and the TPB density measured by using FIB-SEM tomography (marks). In particular, while model predictions and tomography data matched after degradation (i.e., at 200 h), before degradation the L_{TPB} estimated electrochemically from EIS via Eq. (7) was excessively larger than the TPB length evaluated by FIB-SEM tomography. This means that while electrochemical impedance spectroscopy detected all electrochemical degradation, the microstructural evolution of the TPB evaluated with 3D tomography was not sufficient to explain on its own the rapid electrochemical degradation.

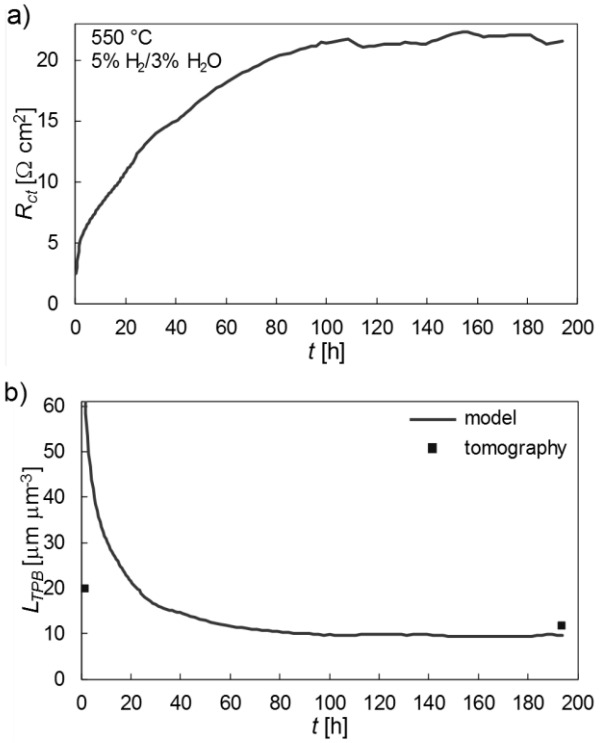

Fig. 4. a) Charge transfer resistance as a function of time of the infiltrated Ni/ScSZ anode as obtained from EIS analysis. b) TPB density as a function of time as estimated from the charge transfer resistance through Eq. (7) (line) and from FIB-SEM tomography (squares).

In order to explain such a mismatch between electrochemical response and microstructural analysis, the TPB line of the sample before degradation was observed at different magnifications, that is, at high resolution by using FEG-SEM (Figure 5a) and at lower resolution through FIB-SEM (Figure 5b). Figure 5a shows that, at high magnification, there are a lot of three-phase boundary points at the Ni/ScSZ interface which could not be resolved by FIB-SEM tomography with a resolution r = 27.2 nm, as shown in Figure 5b. So, the following hypothesis was made [12]: it was assumed that the TPB is rough at the nanoscale, that is, at a length scale which cannot be captured by the finite resolution of 3D tomography. In addition, it was assumed that the evolution of such a nanometric roughness was responsible of the rapid initial electrochemical degradation and of the mismatch of L_{TPB} shown in Figure 4.

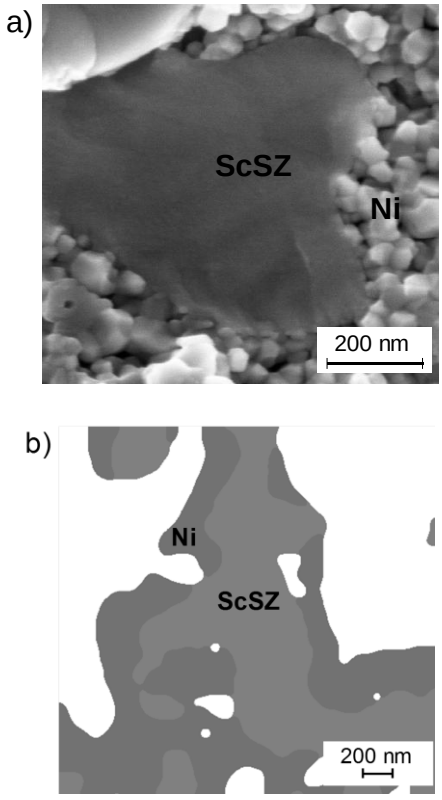

Fig. 5. TPB in a Ni/ScSZ nanostructured anode before degradation at different magnifications: a) FEG-SEM image; b) slice obtained from FIB-SEM tomography after phase segmentation.

In order to corroborate this hypothesis, the roughness of the TPB was quantified by calculating the fractal dimension D of the three-phase boundary according to the Mandelbrot formula [26]. The 3D microstructure was resampled with different voxel sizes r and the TPB density was evaluated at different resolutions as shown in Figure 6a.

Figure 6a shows that the smaller the voxel size r (i.e., better the resolution), the longer the TPB line,

in agreement with the empirical observation made above regarding Figure 5. This means that the TPB is rough at the nanoscale and that the TPB is a fractal in fresh nanostructured anodes [12].

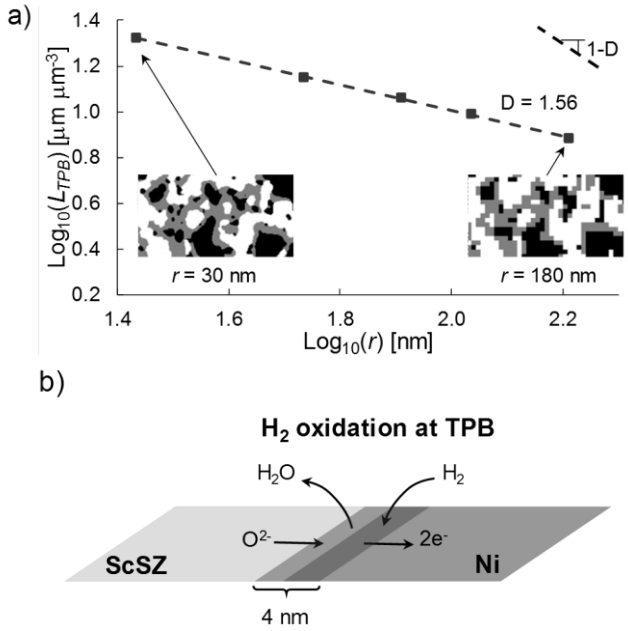

Fig. 6. a) Calculation of the fractal dimension of the TPB by resampling the 3D microstructure of the nanostructured Ni/ScSZ anode before degradation at different resolutions. b) Lateral extension of the reaction zone around the geometrical TPB line at the anode.

However, every fractal in nature is not infinitely rough, that is, there is always a cut-off resolution below which the roughness and nanometric features are not relevant anymore. In the case of the three-phase boundary, such a cut-off resolution must be related to the electrochemistry of the hydrogen oxidation reaction. Therefore, by comparing the TPB density estimated from impedance spectroscopy via Eq. (7) (L_{TPB}^{EIS} = 58.3 μm μm^{-3}, solid line in Figure 4b) and the TPB density measured with FIB-SEM tomography with a voxel size r = 27.2 nm (L_{TPB}^{tomo} = 19.8 μm μm^{-3}, mark in Figure 4b), the cut-off resolution $r_{cut\text{-}off}$ was estimated through the power-law dependence of the fractal TPB shown in Figure 6a, as follows [12]:

$$r_{cut-off} = r \cdot \left(\frac{L_{TPB}^{EIS}}{L_{TPB}^{tomo}} \right)^{1/(1-D)} = 27.2\ \text{nm} \cdot \left(\frac{58.3\ \mu\text{m}^{-2}}{19.8\ \mu\text{m}^{-2}} \right)^{1/(1-1.56)} = 4\ \text{nm} \quad (8)$$

Eq. (8) indicates that the nanometric roughness of the TPB does not affect the charge transfer reaction below 4 nm. This means that 4 nm represents the lateral extension of the hydrogen oxidation reaction zone across the geometrical TPB line, as depicted in Figure 6b. This is in good agreement with mechanistic predictions reported in the literature [27,28], which indicate that the reaction/surface diffusion width of the hydrogen oxidation reaction is in the order of 5 nm. Therefore, it is worth noting that the calculation of the TPB fractal dimension, which is a microstructural property, and its combination with the TPB density estimated by Eq. (7) from EIS data, which encode electrochemical information, provided an independent way to estimate the lateral extension of the anodic reaction around the geometrical TPB line.

Practical implications

The analysis reported in the previous section allowed for the identification of the width of the reaction zone in SOFC composite anodes, which is in the order of 4 nm. Such a lateral extension of the TPB can be neglected when dealing with micrometric particles, situation in which it can be safely assumed that the reaction occurs at the geometrical TPB line. However, this assumption is no longer valid when Ni nanoparticles are present, as in nanostructured electrodes [12,25] and in redox-cycled anodes [29]. Furthermore, the extension of 4 nm sets the minimum resolution requirements to resolve the TPB roughness and charge transfer phenomena in SOFC anodes.

The results shown above indicate that most of the rapid electrochemical degradation in infiltrated Ni-based anodes stems from the coarsening of the nanometric roughness of the three-phase boundary. This implies that the rapid electrochemical degradation can be limited or even prevented by controlling the interfacial properties between Ni and the ceramic scaffold to reduce the evolution of the nanometric roughness. Therefore, it is of fundamental importance to understand the nature of the interaction between Ni and ceramic particles. On the other hand, some strategies suggested in the literature, such as the co-infiltration of ceramic nanoparticles as big as 50 nm as sintering inhibitors [30], are expected to be ineffective because sintering inhibitors are too large when compared to the characteristic length of 4 nm of the TPB roughness.

CONCLUSIONS

This perspective paper summarised the efforts of the authors in investigating the nature of the three-phase boundary in SOFC electrodes and the limitations of assuming that charge transfer reactions take place at the geometrical TPB line. Through an advanced integration of mechanistic

modelling, electrochemical tests via impedance spectroscopy, microstructural analysis via SEM and 3D tomography, the lateral extension of the reaction zone around the geometrical TPB line was assessed in composite SOFC cathodes and anodes for the first time.

For the cathode side, results showed that the oxygen reduction reaction is limited by the adsorption and surface diffusion of oxygen on the electrocatalyst surface while the proper charge transfer process at the TPB is not rate-determining. The characteristic length of the oxygen adsorption/surface diffusion process was found to be in the order of 0.2–0.3 μm for LSM. For the anode, an innovative approach based on the calculation of the fractal dimension of the TPB revealed that the hydrogen oxidation reaction occurs within 4 nm around the geometrical TPB line. In addition, results showed that the evolution of the nanometric Ni roughness is responsible for the rapid electrochemical degradation of nanostructured Ni/ScSZ anodes.

These results highlighted that the common assumption of charge transfer reactions occurring at the mono-dimensional TPB line is fundamentally inappropriate, especially when the size of the particles becomes comparable to the characteristic width of the reaction zone. Considering the extension of the reaction zone around the TPB line reveals the importance of the surface properties of the electrocatalyst and of the wetting between metallic and ceramic phases, with practical implications for material selection, optimisation and control strategies to limit degradation phenomena.

REFERENCES

1. S.C. Singhal, *Solid State Ion.*, **135**, 305 (2000).
2. A.S. Thorel, J. Abreu; S.-A. Ansar, A. Barbucci, T. Brylewski, A. Chesnaud,. Z. Ilhan, P. Piccardo, J. Prazuch, S. Presto, K. Przybylski, D. Soysal, Z. Stoynov, M. Viviani, D. Vladikova *Journal of The Electrochemical Society*, **160(4)**, F360, (2013).
3. S. Presto, A. Barbucci, M. Viviani, Z. Ilhan, S.-A.Ansar, D. Soysal, A.S. Thorel, J. Abreu, A. Chesnaud, T. Politova, K. Przybylski, J. Prazuch, T. Brylewski, Z. Zhao, D. Vladikova, Z. Stoynov, *ECS Transactions*, **25(2)**, 773 (2009).
4. M. Viviani, G. Canu, M.P. Carpanese, A. Barbucci, A. Sanson, E. Mercadelli, C. Nicolella, D. Vladikova, Z. Stoynov, A. Chesnaud, A. Thorel, Z. Ilhan, S.-A. Ansar, *Energy Procedia*, **28**, 182 (2012).
5. D. Vladikova, Z. Stoynov, A. Chesnaud, A. Thorel, M. Viviani, A. Barbucci, G. Raikova, P. Carpanese, M. Krapchanska, E. Mladenova, *International Journal of Hydrogen Energy*, **39(36)**, 21561 (2014).
6. M.P. Carpanese, A. Barbucci, G. Canu, M. Viviani, *Solid State Ionics*, **269**, 80 (2015).
7. J. Xu, X. Zhou, J. Cheng, L. Pan, M. Wu, X.Dong, K. Sun, *Electrochimica Acta*, **257**, 64 (2017).
8. M. Mogensen, S. Skaarup, *Solid State Ion.*, **86-88**, 1151 (1996).
9. V.A.C. Haanappel, J. Mertens, D. Rutenbeck, C. Tropartz, W. Herzhof, D. Sebold, F. Tietz, *J. Power Sources*, **141**, 216 (2005).
10. B. Kenney, M. Valdmanis, C. Baker, J.G. Pharoah, K. Karan, *J. Power Sources*, **189**, 1051 (2009).
11. S. Amitai, A. Bertei, R. Blumenfeld, *Phys. Rev. E*, **96**, 052903 (2017).
12. A. Bertei, E. Ruiz-Trejo, K. Kareh, V. Yufit, X. Wang, F. Tariq, N.P. Brandon, *Nano Energy*, **38**, 526 (2017).
13. Y. Fu, S. Poizeau, A. Bertei, C. Qi, A. Mohanram, J.D. Pietras, M.Z. Bazant, *Electrochim. Acta*, **159**, 71 (2015).
14. M.P. Carpanese, D. Clematis, A. Bertei, A. Giuliano, A. Sanson, E. Mercadelli, C. Nicolella, A. Barbucci, *Solid State Ion.*, **301**, 106 (2017).
15. A. Bertei, M.P. Carpanese, D. Clematis, A. Barbucci, M.Z. Bazant, C. Nicolella, *Solid State Ion.*, **303**, 181 (2017).
16. F. S. Silva, T. M. Souza, *International Journal of Hydrogen Energy*, **42**, 26020 (2017).
17. A. Giuliano, M.P. Carpanese, M. Panizza, G. Cerisola, D. Clematis, A. Barbucci, *Electrochimica Acta*, **240**, 258 (2017).
18. G. Raikova, M. P. Carpanese, Z. Stoynov, D. Vladivkova, M. Viviani, A. Barbucci, *Bulg. Chem. Commun*., **41**, 199 (2009).
19. Z. Jiang, C. Xia, F. Chen, *Electrochim. Acta*, **55**, 3595 (2010).
20. A. Banerjee, O. Deutschmann, *J. Catalysis*, **346**, 30 (2017).
21. A. Banerjee, O. Deutschmann, *ECS Trans.*, **68**, 713 (2015).
22. S. Presto, A. Barbucci, M. P. Carpanese, M. Viviani, R. Marazza, *J. Appl. Electrochem*., **39**, 2257 (2009).
23. S.J. Cooper, A. Bertei, P.R. Shearing, J.A. Kilner, N.P. Brandon, *SoftwareX*, **5**, 203 (2016).
24. A. Bertei, E. Ruiz-Trejo, F. Tariq, V. Yufit, A. Atkinson, N.P. Brandon, *Int. J. Hydrog. Energy*, **41**, 22381 (2016).
25. J. Chen, A. Bertei, E. Ruiz-Trejo, A. Atkinson, N.P. Brandon, *J. Electrochem. Soc.*, **164**, F935 (2017).
26. B. Mandelbrot, *Science*, **156**, 636 (1967).
27. M. Vogler, A. Bieberle-hütter, L. Gauckler, J. Warnatz, W.G. Bessler, *J. Electrochem. Soc.*, **156**, B663 (2009).
28. D.G. Goodwin, H. Zhu, A.M. Colclasure, R.J. Kee, *J. Electrochem. Soc.*, **156**, B1004 (2009).
29. B. Song, E. Ruiz-Trejo, A. Bertei, N.P. Brandon, *J. Power Sources*, **374**, 61 (2018).
30. T. Klemensø, K. Thydén, M. Chen, H.-J. Wang, *J. Power Sources*, **195**, 7295 (2010)..

Нов аспект за ролята на трифазната граница при електроди в твърдо оксидни горивни клетки

А. Бертей[1,2 *], Е. Руиз-Трехо[2], Д. Клематис[3], М.П. Карпанезе[3], А. Барбучи[3], К. Николела[1], Н. Брендън[2]

[1]*Катедра по гражданско и промишлено инженерство, Университет в Пиза, Ларго Луцио Лазарино 2, 56122 Пиза, Италия*

[2]*Катедра по наука за Земята, Имериал колидж Лондон, ул. Принц Конкорд, СВ7 2АЗ Лондон, Великобритания*

[3]*Медицински факултет, Химическо и екологично инженерство, Университет в Генуа, Виа Монтегларо 1, 16145 Генуа, Италия*

Постъпила на 14 май 2018г.; приета на 24 юли 2018г.

(Резюме)

В памет на проф. Здравко Стойнов

В композитни електроди за твърдо оксидни горивни клетки (ТОГК), електрохимичните реакции се осъществяват в близост до така наречената трифазна граница (ТРВ), контактният периметър, където трите фази електрон-проводящи, йон-проводящи и пори се срещат. Строго погледнато, ТРВ е линия и за да се намалят активационните загуби, се налага да се увеличи дължината на тази линия на единица обем от електрода. В настоящата статия, чрез комбиниране на физическо моделиране, 3D томография и електрохимична импедансна спектроскопия (ЕИС) се предлага ново виждане на електродите за ТОГК, което показва, че електрохимичните реакции се осъществяват в разширена област около геометричната ТРВ линия. Тази разширена област е от порядъка на 4 нм в аноди от Ni/$Sc_{0.2}Zr_{0.9}O_{2.1}$ (Ni/ScSZ) и достига стотици нанометри в катоди от $La_{0.8}Sr_{0.2}MnO_{3-x}$/$Y_{0.16}Zr_{0.92}O_{2.08}$ (LSM/YSZ). Тези данни имат съществено значение за предотвратяване на деградацията на наноструктурирани аноди, дължаща се на загрубяване и фрактална грапавост на Ni-те наночастици, както и за оптимизиране на композитни катоди, което показва, че адсорбцията и повърхностната дифузия на кислорода ограничават скоростта на редукция на кислород (РК). Както в аноди, така и в катоди, резултатите показват, че повърхностните свойства на материалите са от ключово значение за определяне на експлоатационните качества и дълготрайност на електродите за ТОГК.